NASA Technical Memorandum 103239

High-Temperature Deformation and Microstructural Analysis for Si3N4-Sc2O3

Deock-Soo Cheong and William A. Sanders
Lewis Research Center
Cleveland, Ohio

NASA

HIGH-TEMPERATURE DEFORMATION AND MICROSTRUCTURAL ANALYSIS FOR Si_3N_4-Sc_2O_3

Deock-Soo Cheong* and William A. Sanders
National Aeronautics and Space Administration
Lewis Research Center
Cleveland, Ohio 44135

ABSTRACT

Limited past studies have indicated that Si_3N_4 doped with Sc_2O_3 may exhibit high-temperature mechanical properties superior to Si_3N_4 systems with various other oxide sintering additives. High-temperature deformation of samples was studied by characterizing the microstructures before and after deformation. It was found that elements of the additive, such as Sc and O, exist in small amounts at very thin grain boundary layers and most of them stay in secondary phases at triple and multiple grain boundary junctions. These secondary phases are devitrified as crystalline $Sc_2Si_2O_7$. Deformation of the samples was dominated by cavitational processes rather than movements of dislocations. Thus, the excellent deformation resistance of the samples at high temperature can be attributed to the very small thickness of the grain boundary layers and the crystalline secondary phase, as suggested earlier.

INTRODUCTION

In 1977 Andersson and Bratton (Ref. 1) investigated the effectiveness of several oxide densification aids for Si_3N_4. They were seeking oxide additives which would yield fully dense hot pressed Si_3N_4 with good strength retention up to 1370 °C. One of 14 oxides evaluated was Sc_2O_3 selected because of its high silicate melting point (Ref. 2). Andersson and Bratton (Ref. 1) were unable to fully densify Si_3N_4 with Sc_2O_3 for strength testing, but suggested that it probably had the greatest potential for high-temperature strength retention. This conclusion was based on the inverse relationships found

---

*National Research Council - NASA Research Associate at Lewis Research Center.

between the ionic radii of rare earth metals in the silicate $M_2Si_2O_7$ with both the 1400 °C flexural strength and the incipient melting point of corresponding $Si_3N_4-M_xO_y-SiO_2$ eutectic mixtures. Ionic radius was selected as a variable since it is indicative of the bond strength of a rare earth silicate with the $M_2Si_2O_7$ structure. The $Si_3N_4-Sc_2O_3-SiO_2$ combination had the highest incipient eutectic point, and Sc had the smallest ionic radius among rare-earth elements. Negita (Ref. 3) pointed out that Sc is one of several metals whose oxides successfully sinter Si_3N_4 where the oxide metal ions have electronegativities less than about 1.5 and ionic radii less than 0.1 nm. It was suggested that ionic materials with these characteristics introduced into the grain boundary phase of a Si_3N_4 material promote faster diffusion and sintering. This improved sinterability results from the introduction of these ionic materials which cause surface energy relaxation owing to the nondirectional and long-range properties of the ionic bond. It was further suggested that based on geometrical considerations, metal ions with radii 0.1 nm can substitute for silicon or migrate in channels parallel to the c-axis in the β-Si_3N_4 structure, also promoting sintering (Ref. 3).

In 1981, Morgan and co-workers (Ref. 4) suggested that Sc_2O_3 might be an appropriate sintering aid for Si_3N_4 since Sc_2O_3 was unlikely to form quaternary metal silicon oxynitrides when added to Si_3N_4. These metal-silicon-oxynitrides can expand upon oxidation causing cracking (Ref. 5). In the work of Morgan et al., $Si_3N_4-SiO_2-Sc_2O_3$ compositions were hot pressed at 1600 to 1800 °C to determine phase relations, and no quaternary phases were found by x-ray diffraction analysis. Subsolidus tie lines were only found to exist between Si_3N_4 and Sc_2O_3, Si_3N_4 and $Sc_2Si_2O_7$, and $Sc_2Si_2O_7$ and Si_2N_2O. A composition of Si_3N_4-18 mol % SiO_2-8 mol % Sc_2O_3 was selected for hot pressing trials and to provide material for oxidation and compressive creep tests, both at 1400 °C.

2

It was found that a 4-hr hold at 1800 °C under 29 MPa pressure was required to nearly complete the $\alpha \rightarrow \beta$ Si_3N_4 phase transformation. Sluggish densification and transformation kinetics were suggested to be indicative of high eutectic temperature within the $Si_3N_4-SiO_2-Sc_2O_3$ system. The composition proved to be very resistant to oxidation at 1400 °C (0.44 mg/cm^2 weight gain in 285 hr), and exhibited 1400 °C compressive creep stress exponents pointing to creep dominated by diffusional processes at stresses less than 275 MPa and dominated by cavitational processes at higher stresses. The likelihood of cavitational processes acting at stresses $\geq$275 MPa was substantiated by a decrease in the density of the test specimen as a result of testing. The creep resistance of the $Si_3N_4-SiO_2-Sc_2O_3$ material was found to be one to two orders of magnitude superior to that of Si_3N_4/MgO materials. Morgan et al. found that the microstructure of their $Si_3N_4-SiO_2-Sc_2O_3$ material consisted of a $\beta-Si_3N_4$ matrix of highly prismatic morphology with a $Sc_2Si_2O_7$ crystalline phase surrounding the $\beta-Si_3N_4$ grains. A very thin (~1 nm) continuous intergranular glassy phase and a few large glass pockets were also noted.

Also in 1981, Dodsworth and Thompson (Ref. 6) conducted studies on the suitability of Sc_2O_3 as a densifier for Si_3N_4. Si_3N_4 with 2 wt % Sc_2O_3 was hot pressed at 1700 °C, but could not be fully densified if pressureless sintered at 1700 °C. Higher temperatures required for densification by pressureless sintering could not be applied due to volatilization of silicon monoxide. Oxidation resistance of hot pressed Si_3N_4 containing 2 wt % Sc_2O_3 for 120 and 100 hr at 1000 and 1400 °C, respectively, was excellent with weight gains of only 0.02 and 0.25 mg/cm^2, respectively. Creep tests of hot pressed Si_3N_4 with 2, 5, and 10 wt % Sc_2O_3 at 1225 °C, 77 MPa showed that creep was enhanced as the level of additive was increased. However, this trend was reversed for the same materials devitrified for 120 hr.

In a study of oxynitride glasses containing scandium, Tredway and Loehman (Ref. 7) found that Sc_2O_3 is thermodynamically compatible with Si_3N_4 based on the formation of oxynitride glasses without decomposition, and that melts can be made in which Si_3N_4 is soluble. Thus, the solution-precipitation sintering mechanism for Si_3N_4 would be operative. Tredway and Loehman pointed out a limited glass forming region for scandium oxynitride glasses and suggested that the intergranular phase in Si_3N_4 sintered with Sc_2O_3 might crystallize more readily than is the case for other sintering additives. Crystallization of the grain boundary glass in sintered Si_3N_4 has been suggested as a technique for increasing high-temperature strength (Ref. 8).

In another study of scandium-containing oxynitride glasses, Mecartney (Ref. 9) found that pieces of hot pressed Si_3N_4 joined with a glass containing Sc_2O_3 showed that scandium had diffused down the grain boundaries of the hot pressed Si_3N_4 and had crystallized as groups of small precipitates in pockets. This occurred without heat treatment. The ready crystallization of the oxynitride glass was absent when Sc_2O_3 was excluded. It was suggested that under appropriate annealing conditions the crystallization of Sc_2O_3-containing grain boundary glasses could be made more uniform and extensive resulting in a sintered Si_3N_4 material with improved creep resistance.

In the present investigation, 2.2 wt % Sc_2O_3 doped Si_3N_4 test bars were deformed in a stepped temperature mode to 1400 °C under various loads, and the microstructural analysis of these samples was performed with TEM, HREM, EDS, x-ray Diffractometry, and SEM. The primary object of this study was to understand the microstructures of the undeformed and the deformed samples and to relate these findings to the observed high-temperature deformation behavior.

EXPERIMENTAL PROCEDURES

Materials and Processing

Si_3N_4[1] (97.7 g) and Sc_2O_3[2] (2.3 g) powders were ground together as a 100-g charge in a 1-liter SRBSN (Sintered Reaction Bonded Silicon Nitride) mill[3] filled with HPSN (Hot-Pressed Silicon Nitride) media[4]. The media charge was 800 g of 1 by 1 cm HPSN cylinders and the grinding fluid was 1/2 liter of pure ethanol. Grinding time was 100 hr. After milling, the powder-ethanol slurry was transferred to a drying apparatus employing a heated water bath and a vacuum connection for removal of ethanol vapor[5]. The powder was further dried in a drying oven at 110 °C. The softly agglomerated powder was then crushed using HPSN hardware and sieved through a 149 μm screen. Specific surface area of the powder determinated by the 3-point BET method was 19.8 m^2/g.

Quantitative chemical analysis of the ground powder gave 3.56 percent oxygen and 0.80 percent carbon. Semi-quantitative spectrographic analysis indicated ppm levels of 1000 Y, 730 Fe, 440 Al, 60 Ca, and 50 Cu. Phase content calculations were based on initial charge composition, Si_3N_4 pickup from the milling hardware, oxygen analysis and reduction of some SiO_2 by carbon assumed to occur during sintering. Phase composition of the powder in weight percent was 93.8 Si_3N_4, 3.8 SiO_2, and 2.4 Sc_2O_3. In mole percent, the composition was 87.7 Si_3N_4, 10.1 SiO_2, and 2.2 Sc_2O_3. Phase analyses of the powders and samples after sintering were done with x-ray diffractometry using Cu-K_α radiation.

---

[1]Kemanord Industrikemi, Engineering Ceramics, P95H Ljungaverk, Sweden (Superior Graphite Co., Chicago, ILL.)
[2]Johnson Matthey, 11216, Seabrook, N.H.
[3]Garrett Ceramic Components Division, Torrance, CA.
[4]Iscar Ceramics, Livonia, MI.
[5]Rotavapor, Prieser Scientific, Louisville, KY.

The sieved powder was pressed into bars at 21 MPa using double-acting tungsten carbide-lined dies. Two lengths of die-pressed bars were pressed, 3.8 and 5.7 cm. The common green bar cross-section was 0.79 by 0.45 cm. Green bars were vacuum sealed in latex tubing and isostatically cold pressed at 414 MPa to a density of 1.80 g/cm^3, 58 percent of the calculated theoretical density[6] of 3.12 g/cm^3.

Weighed and measured bars were sintered 15 at a time in a tungsten cup with a loose-fitting lid in a water cooled double-wall furnace heated with a tungsten mesh element. Bars were separated from one another and the tungsten cup with high purity BN discs. The sintering temperature of 2140 °C was maintained for 4 hr with 5 MPa nitrogen overpressure. The shrinkage during sintering process was uniform at ~18 percent for length, breadth, and thickness, with sinter weight loss of ~3 percent.

Test bars were longitudinally ground with a 400-grit diamond wheel and the four long edges were beveled 0.12 mm. Final test bar dimensions were 3.0 by 0.56 by 0.28 cm for the fast fracture test, and 4.5 by 0.56 by 0.28 cm for the stress rupture test. The density of the machined test bars was 3.18 g/cm^3. This value exceeds that of the theoretical density value of 3.12 calculated based on the law of mixtures assuming the presence of three phases, Si_3N_4, SiO_2, and Sc_2O_3 in the as-ground powder. The density of the grain boundary phase is not known, but to explain the density differences, it is suggested that the specific volume of the grain boundary phase is less than the summed specific volumes of the SiO_2 and Sc_2O_3 phases.

---

[6]Theoretical density was calculated by the law of mixtures for the compounds Si_3N_4, SiO_2 and Sc_2O_3.

Mechanical Testing

Four point flexural strength tests were conducted at a crosshead speed of 0.51 mm/min with inner and outer spans of 9.53 and 19.05 mm, respectively. Room temperature tests were conducted with steel fixtures. Elevated temperature tests were conducted using SiC fixtures in a SiC muffle furnace mounted on a testing machine.[7] All tests were conducted in air.

Four-point flexural stress rupture tests were conducted on lever arm ceramic compression creep test machines.[8] Test bars were loaded under constant dead weight in air in a stepped-temperature exposure mode starting at 1100 °C. Every 24 hr the temperature was raised 100 °C within 5 min and held for 24 hr. At 1400 °C the test bar was held under load at least 72 hr unless failure occurred. Flexural stress rupture fixtures were SiC with inner and outer spans of 19.05 and 38.1 mm, respectively. A creep measurement system included an LVDT displacement transducer with a 3-point extensometer made of Al_2O_3 gaging rods with SiC points. The SiC points contacted the test bar tensile surface at the center and beneath the inner load points. Relative deflection was measured and strain calculated by a data acquisition system. The strain calculation for a test bar in four-point bending assumed a constant radius of curvature between the inner load points. Strain was calculated using the simple relation, $\varepsilon_{max} = 4h \times d/a^2$, where ε_{max} is the maximum strain in the outer fiber, h is the bar thickness, d is the relative deflection of the bar center with respect to the inner load points, and a is the inner span length (Ref. 10). Test temperatures, durations, and applied loads are summarized in Table 1.

---

[7]Instron Corporation, Canton. MA.
[8]Applied Test System Inc., Series 2390, Butler, PA.

Microstructural Characterizations

SEM

In order to study grain morphology, and distributions of grain boundaries and secondary phases, the silicon nitride grains were etched using a plasma etching technique (Ref. 11). Contrary to conventional chemical etching processes, this process etches Si_3N_4 grains in preference to other secondary crystalline or glassy phases. The microstructure of the etched sample was observed with SEM (JEOL 840 operated at 30 kV). The fracture surface of stress rupture bar 3 (Table 1) which failed after 8 min under a load of 350 MPa at 1400 °C was coated with Au, and then studied by SEM.

TEM

Microstructural analyses of samples were performed by using TEM (Philips 400T operated at 120 kV). Foils of deformed and undeformed samples were prepared by following the conventional TEM sample preparation procedures. For an undeformed sample, the microstructure of a cross-section of the bar was investigated. A section perpendicular to the cross-section was also studied in order to fully characterize the microstructure of the sample. Microstructural analysis of deformed samples was conducted on both tension and compression surfaces of samples deformed in four-point flexural stress rupture. When a sample failed, an additional foil was prepared near the fracture surface. The Burgers vector of dislocations was determined by using diffraction contrast (Two Beam Condition) experiments. Since secondary phases at triple junctions were very small, the CBED (Convergent Beam Electron Diffraction) was employed to study the crystal structure of the phase. In addition to BF (Bright Field) imaging, DF (Dark Field) imaging technique was also used to examine continuous amorphous intergranular phase. During TEM sessions, chemical analysis of

Si_3N_4 grains and intergranular phases was performed by EDS (Energy Dispersive Spectrometry), equipped with a SiLi Detector.

HREM

Since grain boundary phases are a critical factor for mechanical properties of Si_3N_4, especially at high temperatures, HREM (JEM 4000EX operated at 400 kV) was employed to study the structure of the matrix, secondary phase, and grain boundary phases. To accurately estimate the thickness of the grain boundary, the foil was tilted so that the electron beam was parallel to the grain boundary. The foil was also oriented so that two grains were in a strong diffracting condition in order to have high contrast lattice fringes.

RESULTS AND DISCUSSION

X-ray diffractometry traces for the starting powder and the sintered sample are shown in Figs. 1(a) and (b). The starting powder was predominantly composed of α-Si_3N_4 (space group, P31c) and a small amount of β-Si_3N_4 (marked by arrows in Fig. 1(a)). The amount of β-Si_3N_4 was ~9 percent, calculated by following the method of Gazzara and Messier (Ref. 12). All the α-Si_3N_4 transformed to β-Si_3N_4 (space group, P6$_3$/m) and a small amount of $Sc_2Si_2O_7$ formed during sintering at 2140 °C for 4 hr under 5 MPa N_2 pressure. The whole spectrum in Fig. 1(b) is from β-Si_3N_4, except two peaks (open arrow) for $Sc_2Si_2O_7$. The first peak (2θ = 28.539°) corresponds to 111 reflections, and the second peak (2θ = 30.548) is from 021 reflections of $Sc_2Si_2O_7$. Microstructural and crystallographic information about $Sc_2Si_2O_7$ will be discussed with the TEM analysis.

The morphologies of Si_3N_4 grains and grain boundary phases were delineated by etching the Si_3N_4 grains. Shown in Fig. 2 are β-Si_3N_4 grains, thin grain boundaries, and a secondary phase at multiple grain boundary junctions of the etched sample. Particularly interesting in this micrograph are the many long

acicular grains of hexagonal cross-section which form interlocking structures. Such interlocking structures can provide toughening by crack deflection, which is the major toughening mechanism of monolithic Si_3N_4 materials (Ref. 13).

The Sc_2O_3-Si_3N_4 material was characterized in fast fracture flexure tests at room temperature and 1370 °C. The results are presented in Table 2 and indicate that the material has a strength of 748 MPa at room temperature, and 496 MPa at 1370 °C. The standard deviations of the strengths are 48 and 44 MPa, respectively. The strength of Sc_2O_3-Si_3N_4 material compares favorably with the fast fracture strengths of Si_3N_4 densified with Y_2O_3, CeO_2, La_2O_3, Sm_2O_3, and ZrO_2 at room temperature and shows some advantage at 1370 °C, as shown in Fig. 3 (Refs. 14 and 15). As listed in Table 1, Sc_2O_3-Si_3N_4 bars were tested in stepped-temperature flexural stress rupture at 1350 °C/300 MPa (bar 9) and 1400 °C/250 MPa (bar 8) for durations of 91 and 96/hr, respectively, without failure. The plastic strains of the test bars were 0.86 and 1.48 percent. However, another test bar failed under a stress of 350 MPa after only 8 min at 1400 °C with a plastic strain of 0.35 percent.

The fracture surface of bar 3 which failed under 350 MPa at 1400 °C was observed with SEM (Fig. 4). The surface was relatively rough at high magnification, showing crack deflection (marked D) and in some cases acicular grain pull-out (marked as P). The roughness of the fracture surface of a material is directly related to the fracture toughness of a material (Ref. 16). The fractull surface roughness implies that the crack-propagation path is longer and thus needs more energy for crack propagation, i.e., tougher material. There are many sites where the crack propagated around large acicular grains (marked D) in Fig. 4. These sites are where large acicular grains protrude from the fracture surface or where there are imprints showing the location of such grains prior to fracture. This is good evidence of crack

deflection. Also apparent in the micrograph is the interlocking grain structure.

Detailed microstructure analyses of undeformed and deformed samples were also performed by using TEM. Figure 5(a) shows the general microstructure of a cross-sectional area of an undeformed bar, and Fig. 5(b) shows an area which is perpendicular to this cross-section. There are no apparent differences between the two microstructures, indicating that the interlocking structures are homogeneous and acicular grains were distributed at random. The sample was very dense except for a few localized areas showing scattered pores. The grains with hexagonal shape are cross-sections of the acicular grains. The cross-section corresponds to the basal plane, (0001), as shown in the diffraction pattern, inset in Fig. 6. Thus β-Si_3N_4 grains grow in a preferred orientation, along the c-axis. The six-sided surfaces of the grains are the prismatic planes of the HCP structure. CBED (Convergent Beam Electron Diffraction) (Fig. 7) showed that secondary phases at multiple junctions were crystalline, and that the crystal structure was monoclinic which was confirmed with XRD results. The CBED analysis consistently demonstrated these results at about 50 other sites. The zone axis of the CBED inset in Fig. 7 is [$\bar{1}12$]. There were no indications of amorphous phases in the samples, but this may be due to the limit of detectibility of TEM. Mecartney (Ref. 9) has suggested that Sc enhances crystallization of the glassy phase in the Sc_2O_3-MgO-Si_3N_4 system. And Tredway and Loehman (Ref. 7) proposed that the intergranular phase in Si_3N_4 with Sc_2O_3 crystallizes more readily than intergranular phases in Si_3N_4 resulting from the use of other additives. Preliminary result of interrupted sintering experiments (Ref. 17) showed that the glassy phase in the Sc_2O_3-Si_3N_4 system crystallizes more easily than that in Y_2O_3-Si_3N_4 system. The secondary phase, $Sc_2Si_2O_7$, is also highly refractory by virtue of a high

eutectic temperature (Ref. 2). Thus the excellent high-temperature mechanical properties for Sc_2O_3-Si_3N_4 material can be attributed to high refractoriness and enhanced crystallization of secondary phases.

Apparent inside the Si_3N_4 grains are many grown-in dislocations. Diffraction contrast experiments showed that the Burgers vectors of dislocations is predominantly [0001]. Some grains showed a very high density of dislocations and larger and/or longer grains tend to exhibit more dislocations in this sample (Fig. 8). Burgers vectors of dislocations in Si_3N_4 determined by other researchers (Refs. 18 to 21) agree with the results obtained in this study. Butler (Ref. 18) and Kossowsky (Ref. 19) reported a Burgers vector of ⟨0001⟩. Lee and Hilmas (Ref. 20) reported Burgers vectors for Si_3N_4 of ⟨0001⟩, 1/3⟨1210⟩, and 1/3⟨1123⟩ in the Y_2O_3-Si_3N_4 system after heat treatment at 1500 °C to crystallize the glass phases with formation of the secondary phase, $Y_2Si_2O_7$. During crystallization and phase transformation of the secondary phase, Si_3N_4 grains deform due to a volume change associated with the phase transformation, and dislocations were formed. Lee and Hilmas attributed the decrease of volume to closer packing of atoms during the phase transformation. Dense dislocation networks and tangles were formed during the heat treatment and annealed out after further heat treatments.

For test bar 8 which experienced the greatest strain, 1.48 percent, the microstructures of two sides, tension (Fig. 9(a)) and compression (Fig. 9(b)), were studied in order to elucidate the deformation behavior of the sample. The significant difference between the two surfaces is the incidence of cavitation. The tension side exhibits many more cavities than the compression side and most cavities exist at triple grain junctions and multiple grain junctions, supporting the mechanism of a cavitational process (Ref. 4) through grain boundary sliding during creep. Kossowsky et al. (Ref. 19) studied the

tensile and creep properties of hot-pressed Si_3N_4, and reported that the deformation at high temperatures, above 1000 °C, is controlled by grain boundary sliding. Morgan et al. (Ref. 4) performed compressive creep tests of hot-pressed Sc_2O_3-Si_3N_4 at 1400 °C and obtained results suggesting that cavitation processes were dominant for stress $\geq$275 MPa by showing a decrease of sample density after the tests. Since the stress used in this study, 250 MPa, was close to that of Morgan et al., the cavitation process, suggested by Morgan et al. (Ref. 4), would be operative. In addition to cavity formation at grain boundary junctions, grain boundary separation was observed on a TEM foil, obtained close to the fracture surface of the failed bar 3 (Fig. 10). Grain boundary separation, occurring by growth of cavities during increasing deformation, finally resulted in sample failure (Ref. 22). Also observed in both the tension and compression sides of bar 8 were dislocations, most of which have a Burgers vector of [0001]. Dislocations in deformed Si_3N_4 samples were observed by earlier investigators (Refs. 18 to 21). There were no noticeable differences in dislocation structures between the two sides of the samples, and these dislocations were also observed in undeformed samples. The microstructures of the two sides of less deformed bars, 7 and 9, were also studied with TEM. The microstructures were similar to those of bar 8. Thus the major mechanisms of creep in this system are cavitation and grain boundary sliding, rather than deformation inside grains.

The structural analysis of grain boundary and secondary phases was extended with HREM. Figure 11 (from bar 8) shows the boundary structure between a Si_3N_4 grain and the secondary phase. The upper grain provides lattice fringes for a secondary phase and the lower grain is a Si_3N_4 grain. Lattice fringe spaces of Si_3N_4 and the secondary phase correspond to 2.53 and 2.68 Å, respectively. The lattice fringes in Fig. 11 are too close to measure

the thickness of the grain boundary. Similarly Morgan et al. (Ref. 4) reported that the thickness of the grain boundary for their $Si_3N_4-Sc_2O_3$ material was ~1 nm. Thus, our HREM showed no apparent evidence of amorphous intergranular phases and extremely thin grain boundaries, which is consistent with our results for TEM. Earlier investigators (Refs. 4 and 9) reported the formation of amorphous (glass) phases involving Sc_2O_3, which were not observed in our samples. The discrepancy can be attributed to differences in composition, sintering temperatures and methods, and other additives. Morgan et al. (Ref. 4) observed amorphous films at grain boundaries. Those glass phases may be retained due to the low sintering temperature, 1600 to 1800 °C. Glass pockets at grain junctions reported by Mecartney (Ref. 9) were formed due to additional additives, Al_2O_3 and MgO.

Chemical analysis of samples was performed with EDS during TEM sessions. Figure 12(a) shows the typical elemental trace for a Si_3N_4 grain. No Sc was detected inside the Si_3N_4 grain. However a very small amount of Sc was observed at grain boundaries of the sample (Fig. 12(b)). For the secondary phase, the intensity of the Sc peak was almost the same as the Si peak (Fig. 12(c)). In some cases, the Sc peaks were smaller than those of Si, which may be caused by overlap of the secondary phases and the Si_3N_4 grains. The intensity of the O peak of the secondary phase is distinct, but there were negligible amounts of O at grain boundaries and in Si_3N_4 grains. The relatively small O peak in this case can be caused by absorption effects in the low energy regions. Therefore, Sc from the additive was mostly detected in grain boundary junctions and formed the secondary phase with SiO_2. Very small amounts of Sc were observed in the thin grain boundaries.

SUMMARY OF RESULTS

1. The major deformation mode in flexural creep testing under 250 MPa at 1400 °C of 2.2 wt % Sc_2O_3-Si_3N_4 material was due to cavitational processes and grain boundary sliding as is the case for other monolithic Si_3N_4 materials rather than deformation of Si_3N_4 grains.

2. Elements of the additives, Sc and O, were concentrated at triple and multiple grain boundary junctions and formed the secondary phases, which were identified as crystalline $Sc_2Si_2O_7$ having the monoclinic structure. No evidence of continuous amorphous phases was obtained with TEM and HREM. A very small amount of those elements were detected at grain boundaries. The grain boundaries between two Si_3N_4 grains, or those between grains and secondary phases are very thin (≤ 1 nm).

3. Many dislocations were observed in samples with and without creep tests. These dislocations have mostly Burgers vector of $\langle 0001 \rangle$. Large and/or long Si_3N_4 grains tend to show more dislocations.

CONCLUSION

Excellent mechanical properties of Si_3N_4 with Sc_2O_3 may be attributed to high refractoriness and crystallization of the secondary phase, and the very thin grain boundaries.

REFERENCES

1. C.A. Andersson and R. Bratton, "Ceramic Materials for High Temperature Turbines", Final Techn. Rep., U.S. Energy Res. Dev. Adm. Contr. Ey-76-C-05-5210, 1977.

2. N.A. Toropov and V.A. Vasil'eva, "Equilibrium Diagram of the Scandium Oxide-Silica Binary System", Russ. J. Inorg. Chem., vol. 7, 1001 (1962).

3. K. Negita, "Ionic Radii and Electronegativities of Effective Sintering Aids for Si_3N_4 Ceramics," J. Mat. Sci. Lett., 4 [4] 417 (1985).

4. P.E.D. Morgan, F.F. Lange, D.R. Clarke, and B.I. Davis, "A New Si$_3$N$_4$ Material: Phase Relations in the System Si-Sc-O-N and Preliminary Properties Studies," J. Am. Ceram. Soc., 64 [4] C-77 (1981).

5. F.F. Lange, "Silicon Nitride Alloy Systems:Fabrication, Microstructure, and Properties," Int. Met. Rev., 247 (1980).

6. J. Dodsworth and D.P. Thompson, "The Role of Scandia in the Densification of Nitrogen Ceramics," pp. 51-61 in Special Ceramics 7. Edited by D. Taylor and P. Popper. The British Ceramic Society, Shelton, Stoke-on-Trent, 1981.

7. W.K. Tredway and R.E. Loehman, "Scandium-Containing Oxynitride Glasses," J. Am. Ceram. Soc., 68 [5] C-131 (1985).

8. A. Tsuge, K. Nishida, and M. Komatsu, "Effect of Crystallizing the Grain Boundary Glass Phase on the High-Temperature Strength of Hot-Pressed Si$_3$N$_4$ Containing Y$_2$O$_3$," J. Am. Ceram. Soc., 58 [7-8] 323 (1975).

9. M.L. Mecartney, "Enhanced Crystallization of a Glassy Phase in Silicon Nitride by the Addition of Scandia," J. Am. Ceram. Soc., 70 [12] C-380 (1987).

10. G.W. Hollenburg, G.R. Terwilliger, and R.S. Gordon, "Calculation of Stresses and Strains in Four-Point Bending Creep Tests," J. Am. Ceram. Soc., 54 [4] 196 (1971).

11. K.N. Siebein and W.M. Lovington, "Plasma Etching of Si$_3$N$_4$," pp. 319-329 in Microstructural Science. Vol. 16. Edited by H.J. Cialoni, M.E. Blum, G.W.E. Johnson, and G.F. VanderVoort. American Elsevier Pub., New York, 1980.

12. C.P. Gazzara and D.R. Messier, "Determination of Phase Contents of Si$_3$N$_4$ by X-ray Diffraction Analysis," Am. Ceram. Soc. Bull., 56 [9] 777 (1977).

13. E. Tani, S. Umebayashi, K. Kishi, and K. Kobayashi, "Gas-Pressure Sintering of Si_3N_4 with Concurrent Addition of Al_2O_3 and 5 wt % Rare Earth Oxide – High Fracture Toughness Si_3N_4 with Fiber-Like Structure," Am. Ceram. Soc. Bull., 65 [9] 1311 (1986).

14. W.A. Sanders and D.M. Mieskowski, "Strength and Microstructure of Sintered Si_3N_4 with Rare-Earth-Oxide Additions," Am. Ceram. Soc. Bull., 64 [2] 304 (1985).

15. W.A. Sanders and D.M. Mieskowski, "Strength and Microstructure of Si_3N_4 Sintered with ZrO_2 Additions," Adv. Ceram. Mater., 1 [2] 166 (1986).

16. K. Matsuhiro and T. Takahashi, "The Effect of Grain Size on the Toughness of Sintered Si_3N_4," pp. 807-816 in Annual Conference on Composites and Advanced Ceramic Materials, 13th, Cocoa Beach, FL., Jan. 15-18, 1989, Ceramic Engineering and Science Proceedings, Vol. 10, July/August 1989.

17. D.-S. Cheong and W.A. Sanders, in progress.

18. E. Butler, "Observations of Dislocations in Beta-Silicon Nitride," Phil. Mag. 21, 829 (1971).

19. R. Kossowsky, "The Microstructure of Hot-Pressed Silicon Nitride," J. Mater. Sci., 8, 1603 (1973).

20. W.E. Lee and G.E. Hilmas, "Microstructural Change in Beta-Si_3N_4 Grains Upon Crystallizing the Grain Boundary Glass," Submitted to J. Am. Ceram. Soc.

21. A.G. Evans and J.V. Sharp, "Transmission Electron Microscopy of Silicon Nitride," in Electron Microscopy and Structure of Materials. Edited by G. Thomas, R.M. Fulrath, and R.M. Fisher. University of California Press, Berkeley, CA, 1977.

22. R. Kossowsky, D.G. Miller, and E.S. Diaz, "Tensile and Creep Strengths of Hot-Pressed Si_3N_4," J. Mater. Sci., 10, 983 (1975).

TABLE I. – STEPPED TEMPERATURE FLEXURAL STRESS RUPTURE TESTS

OF $Si_3N_4-SiO_2-Sc_2O_3$ IN AIR

Test bar number	Stress at tensile surface, MPa	Test duration	Final strain, percent
7	200	24 hr at 1100, 1200, 1300 °C; 72 hr at 1400 °C	1.02 No failure
8	250	24 hr at 1100, 1200, 1300 °C; 96 hr at 1400 °C	1.48 No failure
9	300	24 hr at 1100, 1200, 1300 °C; 91 hr at 1350 °C	0.86 No failure
3	350	24 hr at 1100, 1200, 1300 °C; 0.13 hr at 1400 °C	0.35 Failure

TABLE II. – FLEXURAL STRENGTH OF

$Si_3N_4-Sc_2O_3$ TESTED IN AIR

	R.T.	1370
Test bars	10	10
Average strength, MPa	748	496
Standard deviation, MPa	48	44

(a) Starting powder.

(b) Ground surface of sintered bar.
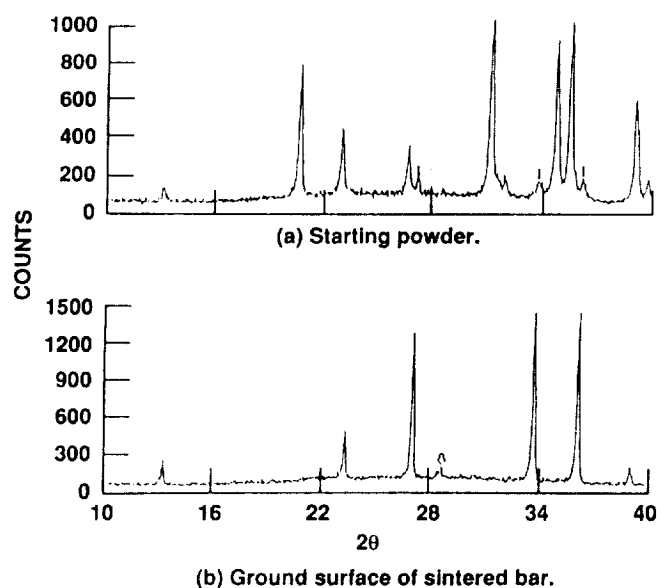
Figure 1.—X-ray diffraction traces for $Si_3N_4-Sc_2O_3$.
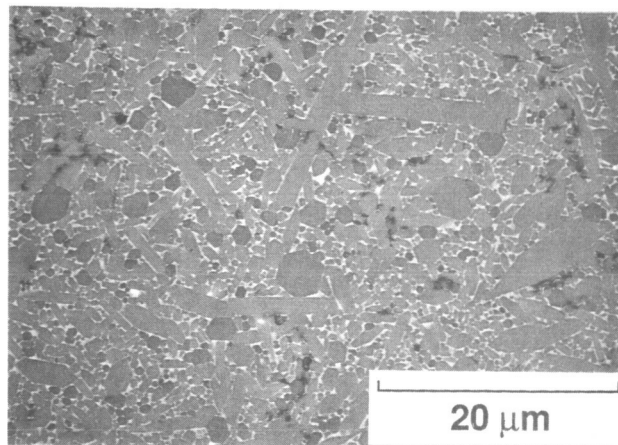
(a) Lower magnification.
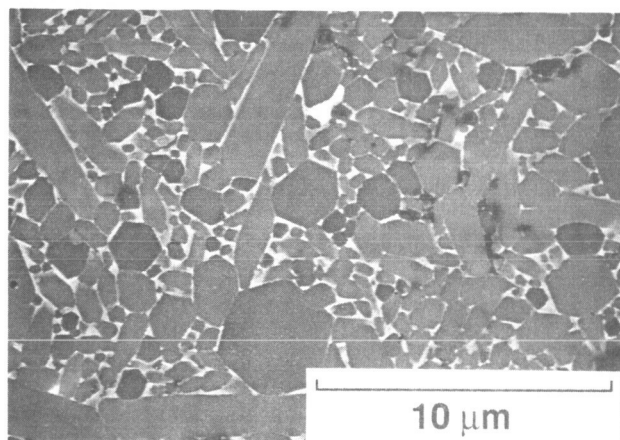
(b) Higher magnification.

Figure 2.—SEM microstructures of plasma-etched Si_3N_4-Sc_2O_3.

M_xO_y
ADDITIVES

○ Y_2O_3
□ CeO_2
◇ La_2O_3
△ Sm_2O_3
I ZrO_2 (4-13 w/o)
+ Sc_2O_3
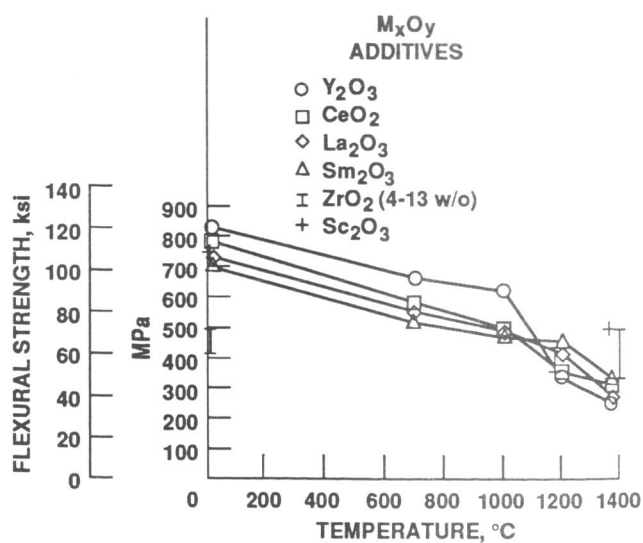
Figure 3.—Flexural strength vs temperature
for Si_3N_4-M_xO_y compositions.
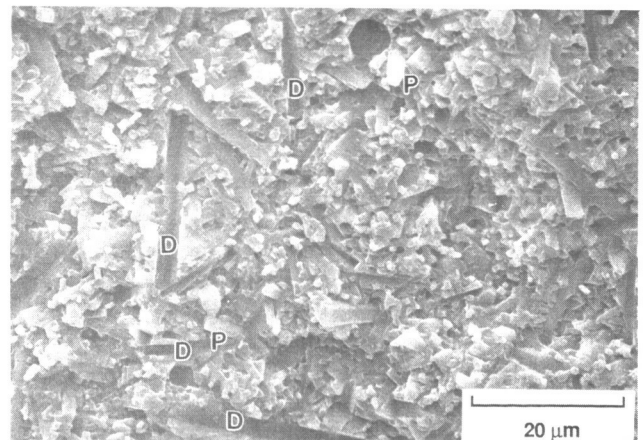
Figure 4.—Fracture surface of stess-ruptured Si_3N_4-Sc_2O_3
(Bar 3) (Noted P; Pull-out acicular grain, D; Crack deflection).

19
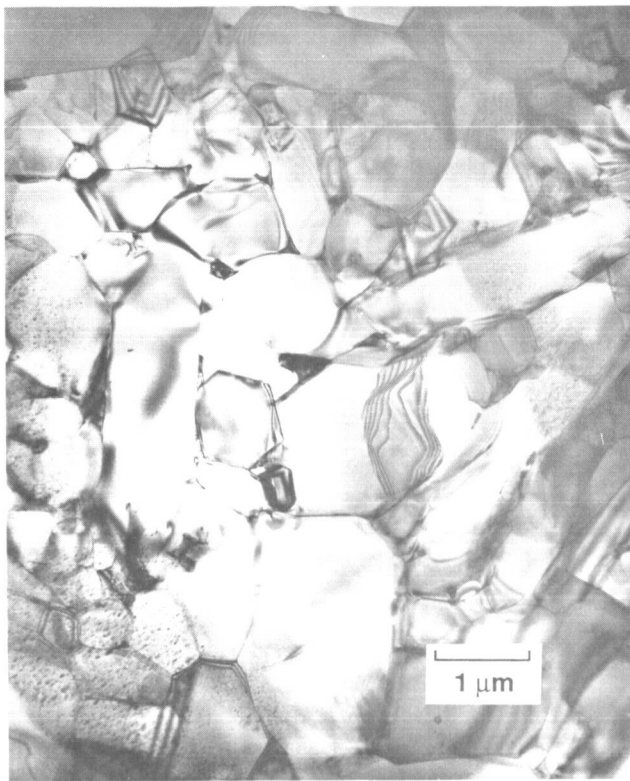
(a) Center of bar cross section.

Figure 6.—TEM micrograph of hexagonal β-Si_3N_4 grain with corresponding diffraction pattern for HCP basal plane (0001).

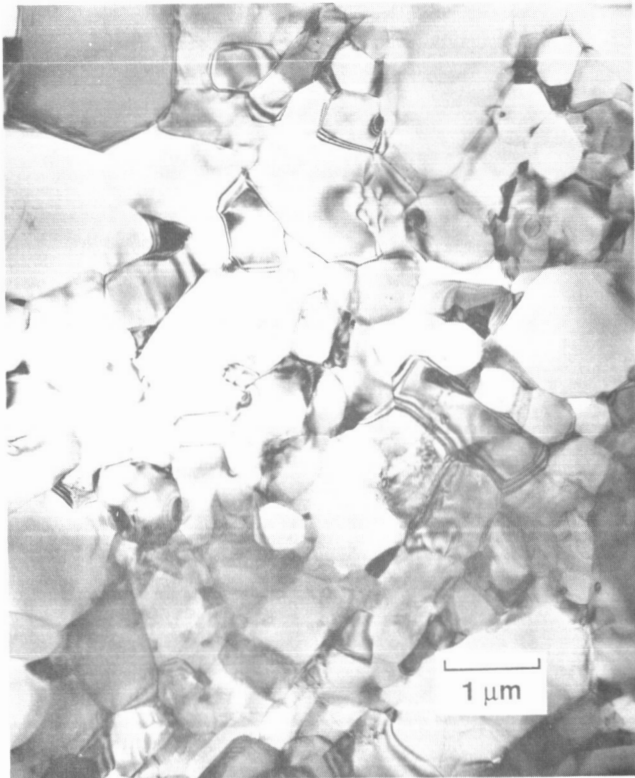(b) Section perpendicular to the cross section.

Figure 5.—TEM micrographs of undeformed Si_3N_4-Sc_2O_3 bar showing similarities.
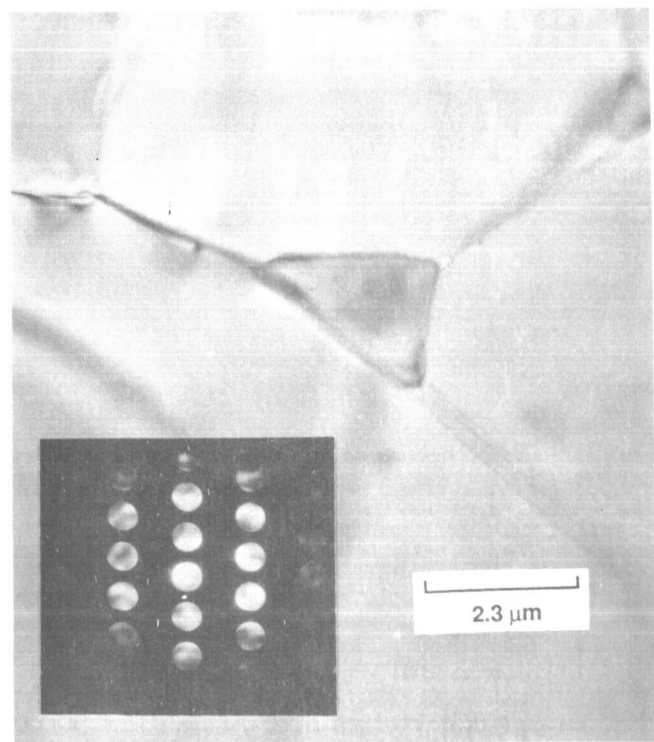
Figure 7.—TEM micrograph with CBED pattern for monoclinic secondary phase at triple point of sintered Si_3N_4-Sc_2O_3.
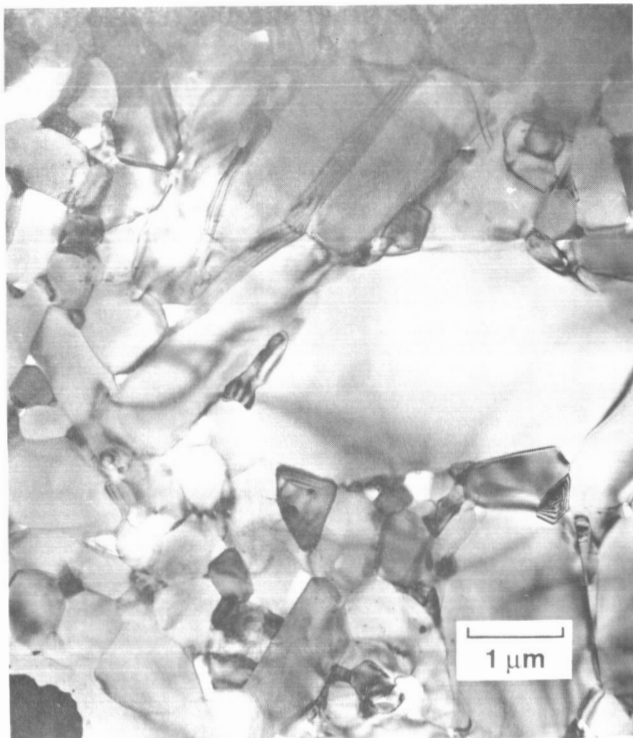
20

Figure 8.—Dislocations in deformed Si_3N_4-Sc_2O_3, having Burgers vector of [0001].
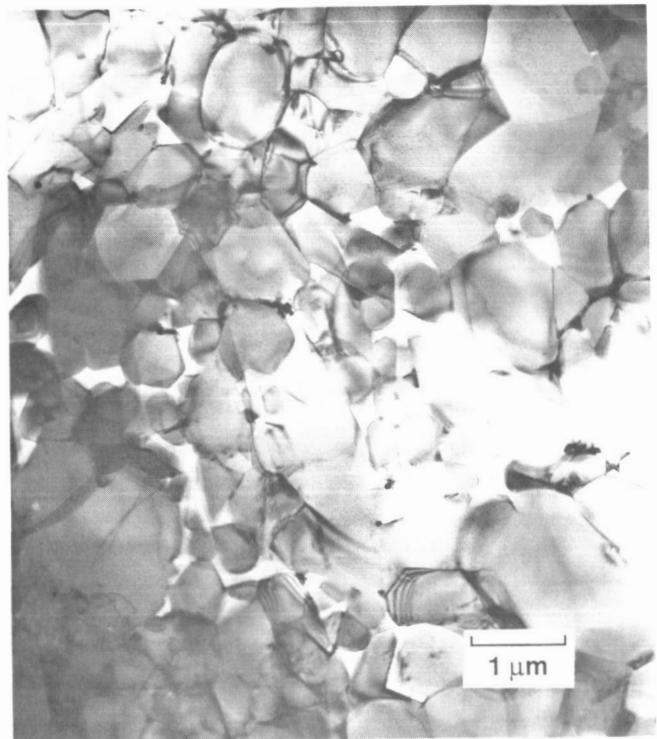
(a) Compressive side.

Figure 10.—TEM micrograph of a foil close to the fracture surface of bar 3, showing grain boundary separation in addition to cavitation.

(b) Tensile side.

Figure 9.—TEM micrograph of deformed Si_3N_4-Sc_2O_3 (ε_p = 1.48 percent).
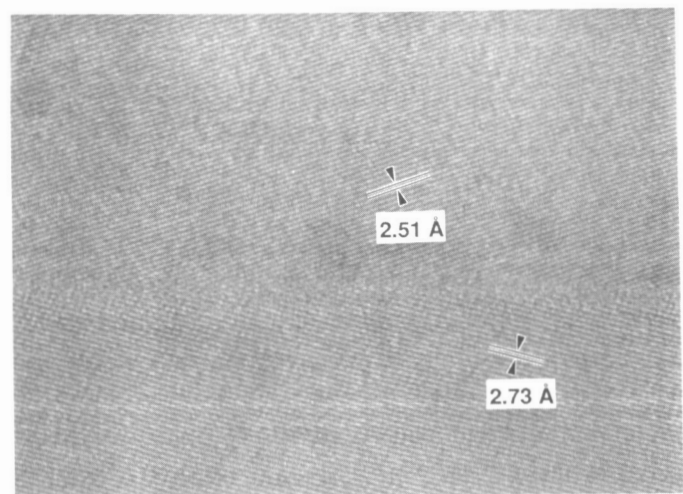

2.51 Å

2.73 Å

Figure 11.—Lattice fringe image of secondary phase (upper grain) and matrix (lower grain). Very thin grain boundary is also between two lattice fringes.
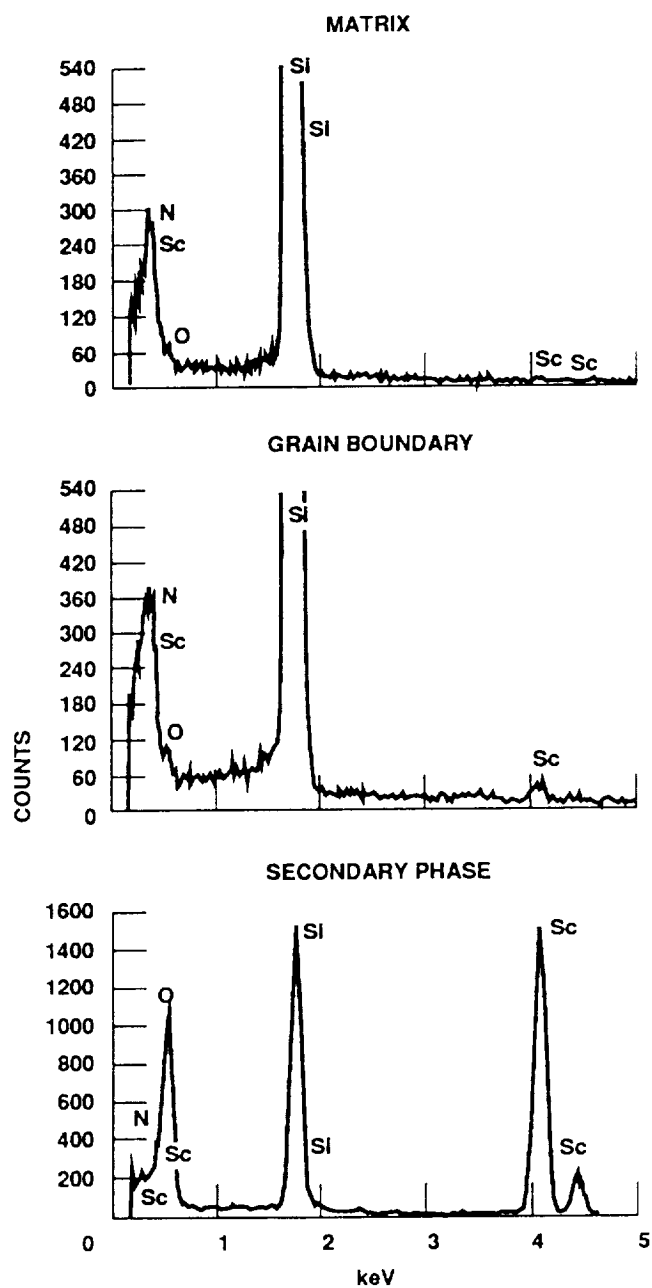
22

Figure 12.—EDS analyses of matrix, grain boundary, and secondary phase.

NASA
National Aeronautics and Space Administration

Report Documentation Page

1. Report No. NASA TM-103239	2. Government Accession No.	3. Recipient's Catalog No.

4. Title and Subtitle High-Temperature Deformation and Microstructural Analysis for Si_3N_4-Sc_2O_3	5. Report Date August 1990
	6. Performing Organization Code

7. Author(s) Deock-Soo Cheong and William A. Sanders	8. Performing Organization Report No. E-5593
	10. Work Unit No. 505-63-1A

9. Performing Organization Name and Address National Aeronautics and Space Administration Lewis Research Center Cleveland, Ohio 44135-3191	11. Contract or Grant No.
	13. Type of Report and Period Covered Technical Memorandum

12. Sponsoring Agency Name and Address National Aeronautics and Space Administration Washington, D.C. 20546-0001	14. Sponsoring Agency Code

15. Supplementary Notes

16. Abstract

Limited past studies have indicated that Si_3N_4 doped with Sc_2O_3 may exhibit high-temperature mechanical properties superior to Si_3N_4 systems with various other oxide sintering additives. High-temperature deformation of samples was studied by characterizing the microstructures before and after deformation. It was found that elements of the additive, such as Sc and O, exist in small amounts at very thin grain boundary layers and most of them stay in secondary phases at triple and multiple grain boundary junctions. These secondary phases are devitrified as crystalline $Sc_2Si_2O_7$. Deformation of the samples was dominated by cavitational processes rather than movements of dislocations. Thus the excellent deformation resistance of the samples at high temperature can be attributed to the very small thickness of the grain boundary layers and the crystalline secondary phase, as suggested earlier.

17. Key Words (Suggested by Author(s)) Si_3N_4-Sc_2O_3 Secondary phase ($Sc_2Si_2O_7$) Grain boundary sliding Cavitation	18. Distribution Statement Unclassified – Unlimited Subject Category 27

19. Security Classif. (of this report) Unclassified	20. Security Classif. (of this page) Unclassified	21. No. of pages 24	22. Price* A03

NASA FORM 1626 OCT 86　　*For sale by the National Technical Information Service, Springfield, Virginia 22161

National Aeronautics and
Space Administration

Lewis Research Center
Cleveland. Ohio 44135

FOURTH CLASS MAIL

ADDRESS CORRECTION REQUESTED

NASA